PHYSICAL REVIEW C **87**, 031306(R) (2013)

Transition probabilities near ^{100}Sn and the stability of the $N, Z = 50$ shell closure

T. Bäck,[1,*] C. Qi,[1] B. Cederwall,[1] R. Liotta,[1] F. Ghazi Moradi,[1] A. Johnson,[1] R. Wyss,[1] and R. Wadsworth[2]
[1]*Royal Institute of Technology, SE-10691 Stockholm, Sweden*
[2]*Department of Physics, University of York, YO10 5DD York, United Kingdom*
(Received 12 April 2012; revised manuscript received 28 February 2013; published 22 March 2013)

Recent $B(E2; 0^+_{\text{g.s.}} \rightarrow 2^+_1)$ measurements in light tin isotopes have revealed surprisingly large values relative to standard shell model predictions, generating an unexpected asymmetry in the $B(E2)$ values with respect to the neutron midshell. This effect has triggered various speculations as to its origin, such as a possible *weakening* of the $N, Z = 50$ shell closure. Here we present new shell model calculations to investigate the origin of the observed asymmetric character of the $B(E2)$ values in the tin isotopes. By including the effects of the neutron $g_{9/2}$ orbital below the $N = 50$ shell gap it is shown that Pauli blocking effects may play an important role near the $N = 50$ shell closure. A new set of single-particle energies and monopole interactions, fitted to the experimental data in the region, together with the isospin-dependent effective charge suggested by Bohr and Mottelson is shown to reproduce the experimental transition rate values in the Sn isotopic chain.

DOI: 10.1103/PhysRevC.87.031306 PACS number(s): 23.20.−g, 21.10.Tg, 21.60.Cs, 27.60.+j

The existence of shell closures for heavy atomic nuclei at the magic numbers 28, 50, 82, and 126, explained by Goeppert-Mayer and Jensen in the 1940s with the introduction of the nuclear spin-orbit coupling, can be considered as one of the cornerstones of nuclear structure physics. However, advances in accelerator and detector technologies have in recent years enabled the study of closed shells far from stability, revealing deviations from the known shell structure in neutron rich nuclei [1]. The structural features of atomic nuclei near the presumed doubly magic shell closure at $^{100}_{50}$Sn$_{50}$ are also of key importance and have therefore attracted the attention of numerous theoretical and experimental studies over several years. This includes measurements and shell model calculations of transition rates in both even-mass [2–6] and odd-mass [7,8] neutron-deficient Sn isotopes, α- and β-decay studies [9–12], and calculations using (quasiparticle) random-phase approximation (Q)RPA models [13–15]. A review of the latest experimental and theoretical advancements in the region of nuclides near ^{100}Sn is given in Ref. [16].

It is recognized that the long isotopic chain of tin isotopes between $N = 50$ and $N = 82$ provides a unique testing ground for nuclear models. Close to the double shell closure at $N = Z = 50$ the shell effects are combined with the enhanced interplay between neutrons and protons moving in the same orbitals. While large experimental advances have been made in the region near ^{100}Sn, the key single-particle and binding energies are still only partly mapped out. Experimental data are lacking even more for transition probabilities, which are generally more difficult to measure than transition energies, but which provide essential details of the nuclear wave function.

The excitation energies of the first 2^+ states between ^{102}Sn and ^{130}Sn have been established [17] and their values are almost constant. This may be understood from the simple perspective of a generalized seniority scheme. However, a series of Coulomb excitation experiments performed at the CERN, GSI, and MSU laboratories have revealed unexpectedly large values of $B(E2; 0^+_{\text{g.s.}} \rightarrow 2^+_1)$ for light Sn isotopes [2–5]. These results were surprising, since it was expected that following the scheme of exact generalized seniority [18,19] the reduced transition probabilities in the Sn isotopic chain would exhibit a symmetry with respect to the neutron midshell. This may indicate that the seniority pairs at the beginning and at the end of the shells have different intrinsic structures [19,20] or that a breaking of the seniority symmetry has occurred. However, shell model calculations have so far not been able to reproduce the large asymmetry in the $B(E2)$ values mentioned above [2–5]. As one approaches the $N = 50$ shell closure, the $B(E2; 0^+_{\text{g.s.}} \rightarrow 2^+_1)$ values should drop rapidly, according to those shell model predictions [2–5]. In contrast, the experimental $B(E2)$ values in even tin isotopes lie almost constant between $N = 62$ and $N = 56$, albeit with large uncertainties, see Fig. 2. These unexpected results have given rise to various speculations, including suggestions of a *weakening* of the $N = Z = 50$ shell closures [5]. Since tellurium ($Z = 52$) lies only two protons above tin in the nuclide chart, $B(E2)$ data for tellurium isotopes, such as the new experimental result for the $N = 56$ nuclide ^{108}Te [21], also provide valuable information for addressing this problem. If the $N, Z = 50$ shell gap energy would be reduced, as discussed in Ref. [5], one would expect significantly enhanced transition probabilities also in light Te isotopes due to the quadrupole interaction between the particles in the $g_{9/2}$ and $d_{5/2}$ subshells. Such an enhancement is not observed experimentally [21]. Further evidence for the robustness of the $N = Z = 50$ shell closure is given by the recent experimental result on the Gamow-Teller strength of β^+ decay of ^{100}Sn [12]. This result was well reproduced by modern shell model calculations.

In the present study we investigate the potential origins of the observed enhanced $B(E2)$ values in the neutron-deficient Sn isotopes. The structural properties of low-lying states in $N = Z$ nuclei just below the $Z = 50$ shell closure can be well described within the relatively isolated $g_{9/2}$ subshell; see, e.g., Refs. [22,23]. Above the shell closure the situation is more complex since an influence of several orbitals is present. The single-particle energies of the $g_{7/2}$ and $d_{5/2}$ orbitals lie

*Corresponding author: back@nuclear.kth.se

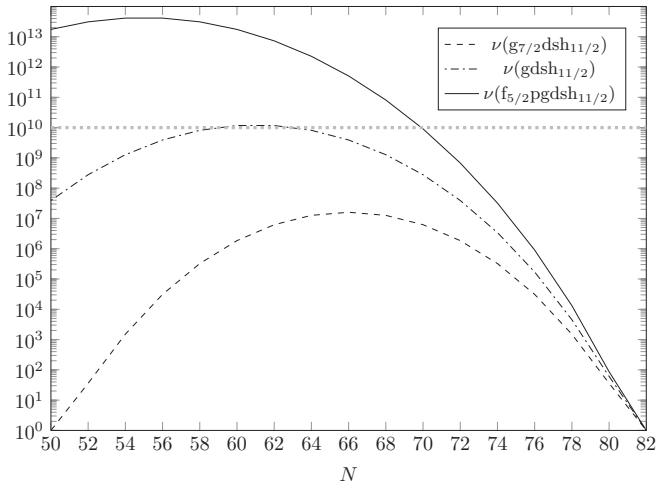

FIG. 1. Shell model dimensions for $M^{\pi} = 0^{+}$ states as a function of the neutron number for the Sn isotopic chain. The dotted horizontal line indicates the present (approximate) computing limit. Including the full neutron model space from $N = 28$ to $N = 82$ ($f_{5/2}$, p, g, d, s, $h_{11/2}$) is beyond today's computer capabilities. The matrix dimension when including both protons and neutrons in the (g,d,s, $h_{11/2}$) model space (not illustrated here) is approximately 10^{18}.

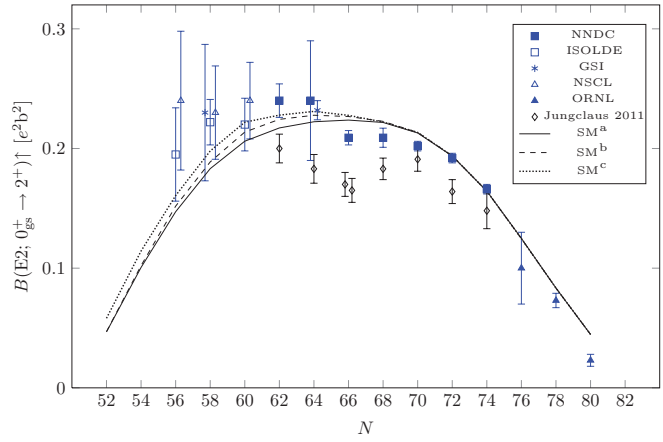

FIG. 2. (Color online) Experimental $B(E2)$ values for Sn isotopes from Refs. [2–6,17,26] and Jungclaus *et al.* [27]. The data are compared with shell model calculations with model spaces involving different combinations of the neutron subshells $g_{9/2}$, $g_{7/2}$, $d_{5/2}$, $d_{3/2}$, $s_{1/2}$, and $h_{11/2}$. SM^{a}: Calculation ($g_{7/2}$, $d_{5/2}$, $d_{3/2}$, $s_{1/2}$, and $h_{11/2}$) with the same ε_{sp} set as in Ref. [2]. SM^{b}: Same as SM^{a} but with inverted ε_{sp} for $d_{5/2}$ and $g_{7/2}$. SM^{c}: Same as SM^{b} but adding the $\nu g_{9/2}$ subshell to the model space. The $B(E2)$ values are enhanced as one approaches $N = Z$ due to the effect of a reduction of Pauli blocking on core excitations across the $N = 50$ shell gap.

close to each other and their relative order has been a subject of debate [9–11]. Given the collective character of the $E2$ transitions, a large shell model space (e.g., $g_{7/2}$, $d_{5/2}$, $d_{3/2}$, $s_{1/2}$, $h_{11/2}$) is a prerequisite for accurate shell model predictions in this region of the nuclide chart. However, the matrix dimension increases rapidly, even beyond today's computing power, as the model space is expanded further, see Fig. 1. As seen in the figure, for extended model spaces the dimension becomes especially large for the neutron-deficient Sn isotopes of interest here.

The shell model $B(E2; 0^{+}_{g.s.} \rightarrow 2^{+}_{1})$ values in the most neutron-deficient Sn isotopes presented in Refs. [2–5] underestimate the experimental results by around 30% for $N < 60$. The asymmetric shape of the experimental $B(E2)$ values with respect to the neutron midshell could not be reproduced even though the $g_{9/2}$ proton orbital *below* the magic $Z = 50$ shell gap was included in the model space [2–5].

To investigate in detail the origin of the asymmetric shape of the experimental $B(E2)$ values, we focused on the neutron model spaces ($g_{7/2}$, d, s, $h_{11/2}$) and (g, d, s, $h_{11/2}$). In the calculations we use the CD-Bonn interaction [24], renormalized by using the perturbation approach of Ref. [25].

In Fig. 2 the results from our shell model calculations (denoted by SM^{a-c}) are compared with the experimental $B(E2)$ data for the even-mass tin isotopes [2–6,17,26,27]. All calculations presented here use a mass-dependent $\hbar\omega$ value according to Blomqvist and Molinari [28]. To facilitate a comparison with Refs. [2–5], the calculations were performed starting with the same set of single-particle energies, ε_{sp}, as in Ref. [2]. This set of ε_{sp} corresponds to the curve labeled SM^{a} in Fig. 2. By exchanging the single-particle energies of the $g_{7/2}$ and $d_{5/2}$ orbitals, following Ref. [9], we obtained the values labeled SM^{b}. Although the relative effect is small, the change from SM^{a} to SM^{b} goes in the right direction towards the experimental values.

In agreement with the calculations presented in Refs. [2–5], we found that *proton* core excitations by themselves could not explain the asymmetric nature of the $B(E2)$ data. More realistic calculations should involve the effects of both neutrons and protons in shells between nucleon numbers 28 and 82. However, this is well beyond the current computational limits, see Fig. 1. To investigate the role played by *neutron* excitations from the $\nu g_{9/2}$ orbital we used the neutron model space (g, d, s, $h_{11/2}$). The corresponding result is denoted as SM^{c} in Fig. 2. This curve contribute to an additional enhancement of the calculated $B(E2)$ values below the neutron midshell. This enhancement can be interpreted in terms of Pauli blocking; the excitation of neutrons from the $g_{9/2}$ orbital into the orbitals directly above the $N = 50$ shell gap is hindered as these orbitals are being filled (i.e., for higher neutron numbers). As seen in the figure, the effect is about 25% of the $B(E2)$ value at $N = 52$ and then decreases as we approach the midshell. This Pauli blocking effect is quite sensitive to the magnitude of the $N = 50$ shell gap and can be enhanced by reducing the gap energy. We have used a constant value for the ($g_{9/2}$, $g_{7/2}$) gap at a realistic energy of 6 MeV; see, e.g., Ref. [29].

The chosen value of the constant effective neutron charge influences the results, but will not affect the asymmetric enhancement of $B(E2)$ values in the light Sn isotopes. For a relevant comparison we have, in all the calculations discussed above, used the same effective charge ($e_{n}^{\mathrm{eff}} = 1.0e$) as in Refs. [2–5].

For the extended calculations including the $\nu g_{9/2}$ subshell, we only take into account multipole two-body interaction matrix elements that can excite one neutron or a neutron

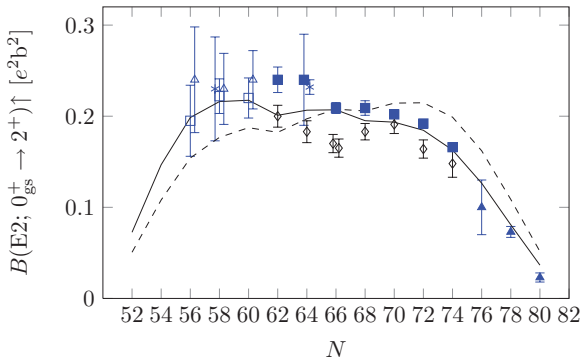

FIG. 3. (Color online) Experimental $B(E2)$ values for Sn isotopes from Refs. [2–6,17,26,27] (same as in Fig. 2) compared to the shell model calculations in the $(g_{7/2}, d, s, h_{11/2})$ model space using the new set of values for $\varepsilon_{\mathrm{sp}}$ fitted from experimental data in the Sn region. The dashed model curve corresponds to a constant neutron effective charge, $e_n^{\mathrm{eff}} = 1.0e$. The solid curve uses the isospin-dependent e_n^{eff} from Bohr and Mottelson [31], normalized to $e_n^{\mathrm{eff}} = 1.0e$ at $N = 66$.

pair from the $g_{9/2}$ orbit to the subshells above $N = 50$. The influence of the monopole interaction that involves the $g_{9/2}$ subshell can be taken into account by keeping the $N = 50$ shell gap energy at a constant value for the entire Sn isotopic chain.

The new experimental results obtained by Jungclaus *et al.* [27] challenge the adopted values in the midshell region and suggest, compared to the adopted values, a more pronounced minimum of $B(E2)$ values around $N = 66$. In Fig. 2, these values are included, together with data from Refs. [3,5,6,17, 26]. We note that the new data follow approximately the *shape* of the NNDC data in the midshell.

As mentioned above, in the calculations discussed so far, we have used the same $\varepsilon_{\mathrm{sp}}$ values as in Ref. [2] (except for the exchange of $\varepsilon_{\mathrm{sp}}$ for $d_{5/2}$ and $g_{7/2}$, see above). The realistic CD-Bonn potential was adopted in the above calculations without any empirical modification. One may suspect that the uncertainties in the Hamiltonian in relation to the uncertain single-particle energies of the shells $s_{1/2}$, $d_{3/2}$, and $h_{11/2}$ and the monopole corrections to the two-body interaction may influence the trend of the calculated $B(E2)$ values. To investigate in detail the role played by the individual single-particle orbitals and to make the best possible choice of single-particle energies we used a new set of $\varepsilon_{\mathrm{sp}}$ and monopole interactions which fit the latest experimental data in the region [30]. This reproduces the experimental low-lying yrast state binding energies within 130 keV in all Sn isotopes and generates the $B(E2; 0^+_{\mathrm{g.s.}} \to 2^+_1)$ values in Fig. 3, dashed curve. A clear asymmetry has now been created with respect to the neutron midshell, but in the opposite direction compared to the experimental data. This shows that the $B(E2)$ asymmetry cannot be reproduced within this model space with a constant effective charge. Moreover, the contributions to the $B(E2)$ asymmetry of SM[b,c] in Fig. 2 are small in comparison to the effects induced by the new $\varepsilon_{\mathrm{sp}}$ set and monopole interactions.

It is well known, see, e.g., Ref. [31], that using constant neutron and proton effective charges, as was done in Refs. [2–5] and as we have done so far, is only an approximation. The polarization effect depends on the individual orbitals as well as on the binding energy of the specific nucleon [31,32]. The effective charge is also expected to depend on isospin. Since $(N - Z)/A$ varies considerably over the long Sn isotopic chain such effects can be important in this case. Bohr and Mottelson [31] deduced an isospin-dependent polarization charge taking isoscalar and isovector polarizabilities and neutron excess into account. They obtained

$$e_{\mathrm{pol}} = \frac{Z}{A} - 0.32\frac{N-Z}{A} + \left(0.32 - 0.3\frac{N-Z}{A}\right)\tau_z, \quad (1)$$

where τ_z is 1 for neutrons and -1 for protons. The effective charge e^{eff} is then the sum of the free nucleon charge and this polarization charge. With this formula the neutron effective charge changes by approximate 30% over the $N = 50$–82 isotopic chain of Sn. In contrast, the proton effective charge is changed by only about 10%. The often used standard values for the effective charges, $e_p^{\mathrm{eff}} = 1.5e$ and $e_n^{\mathrm{eff}} = 0.5e$, correspond to the first term with $N = Z$ in Eq. (1). Using this neutron-number-dependent form for the Sn isotopes and normalizing to $e_n^{\mathrm{eff}} = 1.0e$ at midshell (to account for the proton core excitations) we obtained the solid curve in Fig. 3. One does finally find that the data are well reproduced, including the neutron-deficient region at $^{106-110}$Sn.

In summary, large-scale shell model calculations based on the monopole-corrected CD-Bonn potential have been done to investigate the enhanced $B(E2)$ values below the Sn midshell. Different mechanisms which contribute to the asymmetry (with respect to the neutron midshell) of the $B(E2)$ curve were illustrated. The inclusion of neutron core excitations were shown to induce a Pauli blocking effect which produced a small enhancement of the $B(E2)$ value at the most neutron-deficient Sn isotopes. By fitting single-particle energies to recent experimental data and including an isospin-dependent effective charge, as proposed by Bohr and Mottelsen [31], we successfully reproduced the trends of the known Sn $B(E2; 0^+_{\mathrm{g.s.}} \to 2^+_1)$ systematics.

This work was supported by the Swedish Research Council under Grant Nos. 621-2012-3805, 621-2010-3694, and 621-2010-4723 and by the UK Science and Technology Facilities Council. We acknowledge the computational support provided by the Swedish National Infrastructure for Computing (SNIC).

[1] O. Sorlin and M.-G. Porquet, Prog. Part. Nucl. Phys. **61**, 602 (2008).
[2] A. Banu *et al.*, Phys. Rev. C **72**, 061305(R) (2005).
[3] J. Cederkäll *et al.*, Phys. Rev. Lett. **98**, 172501 (2007).
[4] C. Vaman *et al.*, Phys. Rev. Lett. **99**, 162501 (2007).
[5] A. Ekström *et al.*, Phys. Rev. Lett. **101**, 012502 (2008).
[6] P. Doornenbal *et al.*, Phys. Rev. C **78**, 031303(R) (2008).
[7] D. DiJulio *et al.*, Eur. Phys. Jour. A **48**, 105 (2012).
[8] D. DiJulio *et al.*, Phys. Rev. C **86**, 031302 (2012).
[9] I. Darby *et al.*, Phys. Rev. Lett. **105**, 162502 (2010).
[10] D. Seweryniak *et al.*, Phys. Rev. Lett. **99**, 022504 (2007).
[11] J. Ressler *et al.*, Phys. Rev. C **65**, 044330 (2002).

[12] C. B. Hinke *et al.*, Nature **486**, 341 (2012).
[13] J. Terasaki, Nucl. Phys. A **746**, 583 (2004).
[14] A. Ansari *et al.*, Phys. Lett. B **623**, 37 (2005).
[15] A. Ansari and P. Ring, Phys. Rev. C **74**, 054313 (2006).
[16] T. Faestermann, M. Górska, and H. Grawe, Prog. Part. Nucl. Phys. **69**, 85 (2013).
[17] http://www.nndc.bnl.gov/be2/.
[18] I. Talmi, Nucl. Phys. A **172**, 1 (1971).
[19] I. Morales, P. V. Isacker, and I. Talmi, Phys. Lett. B **703**, 606 (2011).
[20] H. Jiang, Y. Lei, G. J. Fu, Y. M. Zhao, and A. Arima, Phys. Rev. C **86**, 054304 (2012).
[21] T. Bäck *et al.*, Phys. Rev. C **84**, 041306(R) (2011).
[22] B. Cederwall *et al.*, Nature **469**, 68 (2011).
[23] C. Qi *et al.*, Phys. Rev. C **84**, 021301(R) (2011).
[24] R. Machleidt, Phys. Rev. C **63**, 024001 (2001).
[25] M. Hjorth-Jensen *et al.*, Phys. Rep. **261**, 125 (1995).
[26] D. Radford *et al.*, Nucl. Phys. A **746**, 83c (2004).
[27] A. Jungclaus *et al.*, Phys. Lett. B **695**, 110 (2011).
[28] J. Blomqvist and A. Molinari, Nucl. Phys. A **106**, 545 (1968).
[29] A. Blazhev *et al.*, Phys. Rev. C **69**, 064304 (2004).
[30] C. Qi and Z. X. Xu, Phys. Rev. C **86**, 044323 (2012).
[31] A. Bohr and B. Mottelson, *Nuclear Structure*, Vol. II (Benjamin, New York, 1975), Chap. 6, p. 515.
[32] I. Hamamoto and H. Sagawa, Phys. Lett. B **394**, 1 (1997).